

Reactive Molecular Dynamics Simulation of Fullerene Combustion Synthesis: ReaxFF vs DFTB Potentials

Hu-Jun Qian,[†] Adri C. T. van Duin,^{*,‡} Keiji Morokuma,[§] and Stephan Irle^{*,†}

[†]Institute for Advanced Research and Department of Chemistry, Nagoya University, Nagoya 464-8602, Japan

[‡]Department of Mechanical and Nuclear Engineering, Pennsylvania State University, University Park, Pennsylvania 16802, United States

[§]Fukui Institute for Fundamental Chemistry, Kyoto University, Kyoto, 606-8103, Japan

 Supporting Information

ABSTRACT: The dynamic fullerene self-assembly process during benzene combustion was studied using classical Reactive Force Field (ReaxFF) nonequilibrium molecular dynamics (MD) simulations. In order to drive the combustion process, the hydrogen to carbon (H/C) ratio was gradually reduced during the course of the MD simulations. Target temperatures of 2500 and 3000 K were maintained by using a Berendsen thermostat. Simulation conditions and hydrogen removal strategies were chosen to match closely a previous quantum chemical MD (QM/MD) study based on the density-functional tight-binding (DFTB) potential (Saha et al. *ACS Nano* **2009**, *3*, 2241) to allow a comparison between the two different potentials. Twenty trajectories were computed at each target temperature, and hydrocarbon cluster size, C_xH_y composition, average carbon cluster curvature, carbon hybridization type, and ring count statistics were recorded as a function of time. Similarly as in the QM/MD simulations, only giant fullerene cages in the range from 155 to 212 carbon atoms self-assembled, and no C_{60} cages were observed. The most notable difference concerned the time required for completing cage self-assembly: Depending on temperature, it takes between 50 and 150 ps in DFTB/MD simulations but never less than 100 ps and frequently several 100s ps in ReaxFF/MD simulations. In the present system, the computational cost of ReaxFF/MD is about 1 order of magnitude lower than that of the corresponding DFTB/MD. Overall, the ReaxFF/MD simulations method paints a qualitatively similar picture of fullerene formation in benzene combustion when compared to direct MD simulations based on the DFTB potential.

I. INTRODUCTION

Since the discovery of buckminsterfullerene C_{60} (BF),¹ fullerenes have been the focus of research due their unique structures, chemistry, and potential applications in nanotechnology. Historically, fullerenes were synthesized on the gram scale by evaporating carbon atoms from graphite at high temperatures on the order of several thousand Kelvin.^{1,2} Nowadays, industry-scale production of fullerenes is achieved by continuous combustion synthesis in low-pressure fuel-rich flames of certain hydrocarbons.^{3–7} This technique is sensitive to operating conditions, such as fuel type,⁶ fuel/oxygen ratio, temperature, pressure in the combustion chamber,^{4,7} and even chamber design.⁸ Although considerable advances have been made in optimizing the synthesis conditions on a phenomenological basis,⁹ the elementary reaction mechanisms involved in the self-assembly of fullerene cages are still subject to investigation.¹⁰

Experimentally, combustion of hydrocarbon fuels in oxygen-lean flames was found to produce substantial amounts of polycyclic aromatic hydrocarbons (PAHs), which are presumed to be the precursors of fullerenes.^{7,9–14} However, the molecular structures of the intermediate PAH species with more than ~10 carbon atoms remain largely unknown. Experimentally, temperature/profiles, fuel/oxygen ratio as a function of distance from the burner, and *in situ* mass spectra have been recorded. A combination of these data with thermodynamic considerations and kinetic modeling only indirectly sheds light on the PAH H/C ratio as a function of time evolution. On the basis of the recorded

H/C ratio of PAHs in acetylene flames, Homann proposed a picture of “ordered” growth of PAHs along a pathway involving only maximally condensed and fully hydrogenated graphene-like platelets.¹⁰ However, the assumption that such species dominate the aggregation process is only based on thermodynamic stability arguments and neglects entropic effects that are important due to the high environmental temperature. To date, there is no proof that thermodynamically maximally stable species as proposed by Homann and others are true intermediate species in the dynamic fullerene cage self-assembly.

Atomic-scale modeling of complex reaction systems *in silico* has become a useful tool of study, capable of reproducing fullerene self-assembly from benzene, atomic carbon, and C_2 molecules in computer simulations.^{15–22} Over the past six years, Irle, Morokuma, and co-workers have discovered and elaborated on a “shrinking hot giant” (SHG) road of fullerene formation, based on direct quantum chemical molecular dynamics simulations (QM/MD) using a density-functional tight-binding (DFTB) potential.¹⁷ According to the SHG road, the fullerene formation process follows two stages: (1) self-assembly of giant fullerenes (GFs) via a “size-up” process, followed by (2) a shrinking process (termed “size-down”) by irreversibly evaporating C_2 units from vibrationally excited, highly unstable and defective cages. The shrinking process has experimentally been recorded in an *in situ*

Received: March 22, 2011

Published: May 31, 2011

HRTEM movie sequence.²³ Regarding the preceding “size-up” stage, no direct confirmation from experimental results is available. DFTB/MD simulations of pure carbon vapor systems predict three consecutive steps:¹⁶ (1) polyyne chain formation (σ -bond formation between small linear carbon chain fragments) and nucleation of a pentagon/hexagon network into “octopus”-like bowl structures with polyyne “antennas” attached to their openings, (2) ring condensation growth at the bowl openings, and (3) GF cage closure by saturation of dangling bonds at edges, leaving antennas attached to sp^3 cage defects. DFTB/MD simulations of the benzene combustion process by hydrogen removal¹⁵ predicted the following steps: (1) radical creation and ring-opening/fragmentation, (2) growth of polyacetylene-like chain structures, akin to the polyyne chain formation process in pure carbon simulations, followed by a (3) ring condensation process and (4) cage closure. Here, ring condensation was found to ensue after a significant fraction of hydrogen was stripped from the chains, since only then can carbon avoid disruption of favorable conjugation through sp^2 carbons. As a consequence, ring condensation in combustion occurred later than in carbon-only systems, typically after the cluster size was already determined in the hydrocarbon oligomerization process, leaving not a lot of free carbon species to regrow chains at the cluster boundaries. Therefore, GF antennas were formed less frequently in the case of combustion in comparison to carbon-only simulations.

The DFTB method has allowed the direct MD study of the self-assembly process of fullerenes with approximate density functional theory (DFT) accuracy for up to several hundred picoseconds. However, this time scale is still much shorter compared to experimental fullerene synthesis time scales, which occurs on the order of microseconds. Moreover, fullerene synthesis by benzene combustion requires the presence of O_2 molecules for hydrogen abstraction, which occurs only on the order of several hundred picoseconds.^{24,25} Saha et al. had therefore resorted to randomly removing H atoms during the MD, simulating in this way the decreasing H/C ratio during combustion.¹⁵ On the other hand, the semiclassical reactive force field (ReaxFF) method by van Duin and co-workers²⁶ is apparently computationally much more economical and enables the simulation of combustion processes on a nanosecond time scale.^{24,25} The computational efficiency of ReaxFF is paid for by the fact that the force field is local beyond a four-body interaction term and therefore does not explicitly describe resonance structures. Therefore, formally, the famous Hückel aromaticity and Clar²⁷ rules, which are important for the relative stability of PAH isomers, cannot be accurately represented in the ReaxFF potential. We note that in practice, ReaxFF energetics of π -conjugated species are generally in good agreement with quantum chemical DFT benchmark data by virtue of their empirical parametrization.²⁸ However, a systematic comparison of fullerene growth as described by a quantum chemical and a classical potential has never been directly performed. The main goal of this work is therefore to compare ReaxFF/MD with previous DFTB/MD simulations regarding the respective mechanism of fullerene formation during combustion simulations and the computational cost associated with these methods.

II. COMPUTATIONAL METHODOLOGY

ReaxFF is a general bond-order-dependent force field method fitted to potentials derived from first principles DFT calculations,

allowing chemical reactions to take place *via* the cleavage or formation of covalent chemical bonds during a MD run. Atomic bond orders are computed on the fly from the atomic connectivity matrix, with updates at every MD time step. The potential is adjusted as a function of these bond orders, similar as in Tersoff–Brenner type potentials.^{29–31} Nonbonded interactions (van der Waals and Coulomb interactions) are calculated between every pair of atoms, irrespective of connectivity, while a shielding term is introduced for short distances. A full description of the derivation and parametrization in the ReaxFF method is given in refs 24 and 26.

All simulations were performed under constant temperature and constant volume (NVT) conditions, where we maintained target temperatures of 2500 and 3000 K by employing a Berendsen thermostat with a weak coupling constant of $\tau = 100$ ps. This thermostat is closest to, although not identical with, the velocity-scaling thermostat that was employed in our previous DFTB simulations. A relatively short time integration interval of $\Delta t = 0.1$ fs was chosen in the velocity Verlet algorithm to ensure the smoothness of the ReaxFF potential at the employed high temperatures, because in reactive force fields a switching function needs to be frequently updated to handle changes in atomic coordination numbers and corresponding changes in the potential energy. Since the DFTB method does not require a bond order switching function, MD simulations performed on this potential can tolerate a larger time step. For comparison, in the previous DFTB/MD simulations, a time integration interval of $\Delta t = 0.48$ fs had been employed. We adopted the same hydrogen removal strategy as in ref 15, and the initial Cartesian coordinates of benzene molecules are identical as well. In this geometry called g1, 36 benzene molecules are stacked in four layers of nine molecules arranged in a 3×3 quadratic plane within a cubic simulation box with an initial edge length of 21 Å. The interlayer distance was set to 3.4 Å, and the closest intermolecular H contacts are 2.2 Å. Periodic boundary conditions (PBC) were applied on the basis of this cubic unit cell. Using the g1 geometry as a reference, Saha et al. created the three other geometries g2, g3, and g4 by varying interlayer distances. However, the authors mention that the exact initial coordinates of individual benzene molecules have little influence on the trajectories due to rapid randomization of positions at the high temperatures, and thus we only employed the geometry labeled “g1” in this study.

For each temperature, 20 trajectories were simulated starting from the same geometry “g1” with different random H removal sequences. Trajectories are labeled either “2500K_n” or “3000K_n” to distinguish temperature and trajectory number “n”, ranging from 1 to 20. As in the previous DFTB/MD simulations, the combustion process was simulated by a programmed H atom removal process with a random removal rate of 70 hydrogen atoms every 5 ps. This means that for each trajectory, the first H removal process was performed after 5 ps of equilibration, followed by the second and third H removals at 10 and 15 ps. On the occasion of each H removal process, free H atoms/ H_2 molecules (isolated H atoms without any covalent bonds to C atoms) were also removed from the system. At a simulation time of 20 ps, any H remaining in the systems was also removed, and the system was annealed for 500 additional picoseconds. In the previous DFTB/MD simulation, it was found necessary to increase the simulation box edge size from 21 Å to 30 Å after the third H removal at 15 ps because the main cluster size was found to approach the size of the PBC box in

Table 1. ReaxFF/MD Trajectories at 2500 K^a

trajectories	H's removed			t_f/t_{end} (ps)	#C _{cage}	#C _{cluster}	$\langle\langle C^2 \rangle\rangle^{1/2}$ (1/Å)
	@5 ps	@10 ps	@15 ps				
2500K-1	70	70	70	520	212	214	0.232
2500K-2	70	70	70	520	186	216	0.235
2500K-3	70	70	70	674	188	209	0.209
2500K-4	70	70	70	370	158	179	0.260
2500K-5	70	70	70	700.5	186	214	(0.262)
2500K-6	70	70	70	370.5	180	214	(0.237)
2500K-7	70	70	70	630	181	190	0.226
2500K-8	70	70	70	711	172 (open)	203	(0.278)
2500K-9	70	70	70	520	182 (defective)	214	(0.250)
2500K-10	70	70	70	520	183 (defective)	214	(0.237)
2500K-11	70	70	70	268	155	170	0.251
2500K-12	70	70	70	470	176	203	0.240
2500K-13	70	70	70	520	194	216	0.238
2500K-14	70	70	70	520	186 (defective)	214	0.236
2500K-15	70	70	70	520	159 (defective)	202	0.260
2500K-16	70	70	70		unsuccessful	216	
2500K-17	70	70	70		unsuccessful	216	
2500K-18	70	70	70	503.5	191	216	0.239
2500K-19	70	70	70	520	169 (defective)	212	(0.243)
2500K-20	70	70	70	489	184	211	0.263
average ^a				503	183	204	0.241

^aThe last row records the average values of t_f , #C_{cage}, #C_{cluster}, and $\langle\langle C^2 \rangle\rangle^{1/2}$ over all successfully formed cages. t_f corresponds to time of closed cage formation in the successful cases, and t_{end} is the point when the simulation is terminated in the unsuccessful cases. #C_{cage} is the number of carbon atoms in the cage only, and #C_{cluster} is the number of total carbon atoms in the largest cluster at the time of cage formation. $\langle\langle C^2 \rangle\rangle^{1/2}$ is the root mean square (RMS) curvature of the cluster, where curvature C is defined as the inverse radii of spheres best fitted to an sp²-carbon atom plus its three bond neighbors. Brackets $\langle \dots \rangle$ denote an average over sp²-carbons. “Defective” denotes a defective cage is formed, and “open” denotes an open cage.

most of the simulated trajectories, preventing fullerene cage formation due to the formation of an extended graphitic sheet across periodic boundaries. Therefore, the carbon density of the model system was initially 0.46 g/cm³ during the first 15 ps of the trajectories and 0.16 g/cm³ afterward. However, for the ReaxFF/MD simulations presented here, we found that we had to employ an even larger box with 50 Å edge length after 15 ps to prevent graphitic sheet formation due to structure formation across periodic images. The previous DFTB/MD trajectories were computed up to 220 ps simulation time. The present ReaxFF/MD simulations were computationally significantly less expensive, allowing us to follow trajectories up to 700 ps.

III. RESULTS AND DISCUSSIONS

III.A. Self-Assembled Giant Fullerenes. Tables 1 and 2 present the size (# of carbon atoms) of the final formed largest clusters and cages at both temperatures of 2500 and 3000 K, respectively. We note the relatively frequent occurrence of partially nested or spiroid-like structures, which are labeled “defective”. In all cases, we recorded the number of hydrogen atoms randomly removed after 5.0, 10.0, and 15.0 ps. Unlike in previous DFTB/MD simulations, free hydrogen atoms were frequently formed and removed, yet only a single free H₂ molecule was found in trajectory 3000K_9 at 10 ps (Table 2). At 2500 K, 12 out of 20 trajectories formed closed cage structures (GFs) during the simulation time, equivalent to a fullerene yield of 60%. Six of them were found to yield defective or partially open

cages (see the corresponding Cartesian coordinates in the Supporting Information, Tables S1 and S2). At 3000 K, the fullerene yield was even higher with 17/20 = 85% successfully formed GFs. In all successful trajectories, we recorded the time when the closed fullerene cages are formed t_f , the number of carbon atoms both in the cage structure #C_{cage} and in the whole cluster #C_{cluster} at time t_f , and the root-mean-square (RMS) curvatures calculated from the carbon atoms belonging to the largest cluster. The RMS curvature is an average over all of the sp² carbon atoms in the cluster. Similar to that in previous DFTB/MD simulations, we found that a higher temperature favors the formation of smaller cages: #C_{cage} at 2500 K is distributed between 155 and 212 (DFTB/MD: 174–212) with an average of 183 (DFTB/MD: 191), while the cage size at 3000 K is distributed between 157 and 199 (DFTB/MD: 74–201) with an average of 178 (DFTB/MD: 161). Consequently, RMS curvatures are very similar for ReaxFF/MD and DFTB/MD simulations. The number of carbons contained in exohedrally attached polyyne chains (so-called “antennas”) is given as the difference between #C_{cluster} and #C_{cage} in Tables 1 and 2. The average number of antenna carbons is 21 at 2500 K (DFTB/MD: 7) and 16 at 3000 K (DFTB/MD: 25). The successfully formed cages of this study are displayed in Figures 1 and 2 for 2500 and 3000 K, respectively. They occasionally contain endohedrally encapsulated small C_n chains or rings, marked by yellow color, which were not found in our previous DFTB/MD simulations. However, previous tight-binding-based MD³² and reactive force field MD²¹ simulations also predicted similar endohedrally encapsulated carbon clusters.

Table 2. ReaxFF/MD Trajectories at 3000 K^a

trajectory name	H's removed			t_f/t_{end} (ps)	#C _{cage}	#C _{cluster}	$\langle\langle C^2 \rangle\rangle^{1/2}$ (1/Å)
	@5 ps	@10 ps	@15				
3000K_1	70	70	70	264	173	212	0.241
3000K_2	70	70	70	265.5	168	177	0.215
3000K_3	70	70	70	289.5	199	212	0.240
3000K_4	70	70	70	291.5	170	205	0.232
3000K_5	70	70	70	305.5	181	196	0.239
3000K_6	70	70	70	380	184	195	0.226
3000K_7	70	70	70	221.5	168	182	0.224
3000K_8	70	70	70	234.5	181	189	0.232
3000K_9	70	2/70 ^c	70	484.5	182	192	0.250
3000K_10	70	70	70	353	185	202	0.236
3000K_11	70	70	70	410	186	201	0.227
3000K_12	70	70	70	454.5	183	198	0.230
3000K_13	70	70	70	236.5	175	194	0.250
3000K_14	70	70	70	305	157	174	0.232
3000K_15	70	70	70	254	176	202	0.236
3000K_16	70	70	70	423	175	183	0.219
3000K_17	70	70	70	520	190 (open)	212	0.215
3000K_18	70	70	70	520	177 (PAH)	210	0.214
3000K_19	70	70	70	520	163 (PAH)	201	0.227
3000K_20	70	70	70	431.5	182	186	0.237
average ^b				329.6	178	194	0.233

^a Listed quantities have the same meaning as in Table 1. ^b Refer to Table 1. ^c One hydrogen molecule (2 H atoms) was found and removed at 10 ps in the second H removal step in this trajectory.

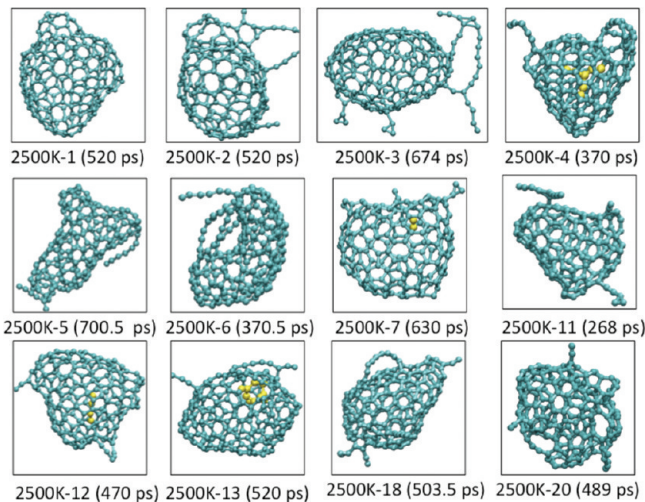


Figure 1. GF cages at 2500 K from the 12 successful trajectories. Yellow spheres indicate encapsulated fragments inside the formed cage.

Similar as in previous DFTB/MD simulations, the cage closure time also depends on the temperature: The average t_f at 2500 K was 503 ps (DFTB/MD: 82), while at 3000 K it was 329.6 ps (DFTB/MD: 46 ps). The most striking difference between DFTB/MD and ReaxFF/MD simulations is the much longer time required for cage formation time in the case of the latter. After 220 ps in ReaxFF/MD (the longest DFTB/MD simulation runs), not a single GF had formed. The reason for this significant discrepancy between ReaxFF and DFTB will be discussed below.

III.B. Dynamics of Giant Fullerene Self-Assembly. In the following sections, we analyze the general properties and processes (key events) of fullerene cage formation for both temperatures. Successful trajectories at the same temperatures followed qualitatively similar patterns, although t_f differed substantially between them. We here discuss only one representative trajectory for each temperature, namely, trajectories 2500K-1 and 3000K-2. Other trajectories follow similar time evolution patterns, although the detailed processes are of course different.

Figure 3 displays the evolution of the potential energy during the course of these trajectories. Discontinuous jumps up in the potential energy curves mark the H removal at 5, 10, and 15 ps, followed by relaxation associated with a potential energy decrease. The potential energy evolution on such a scale was similar to our previous DFTB/MD simulations.

III.B.1. Cluster Growth. Figure 4 displays for both trajectories a histogram of #C_{cluster} sizes of all occurring clusters, where different colors indicate separate molecular clusters. During the initial 5 ps equilibration, no chemical reactions occurred. This is in stark contrast to our previous DFTB/MD study, where pyrolytic H abstraction and radical reactions were observed, particularly at the higher temperature. At both low and high temperatures, the growth of the largest cluster started dramatically after the first H removal at 5 ps but slowed down after all the H atoms were removed from the system after 20 ps. At this time, a large cluster comprised of about half (2500K-1) or less than half (3000K-2) the number of carbon atoms had formed along with a couple of other, smaller clusters. In contrast, the apparently more reactive DFTB/MD simulations exhibited already after 20 ps a cluster consisting of almost all available

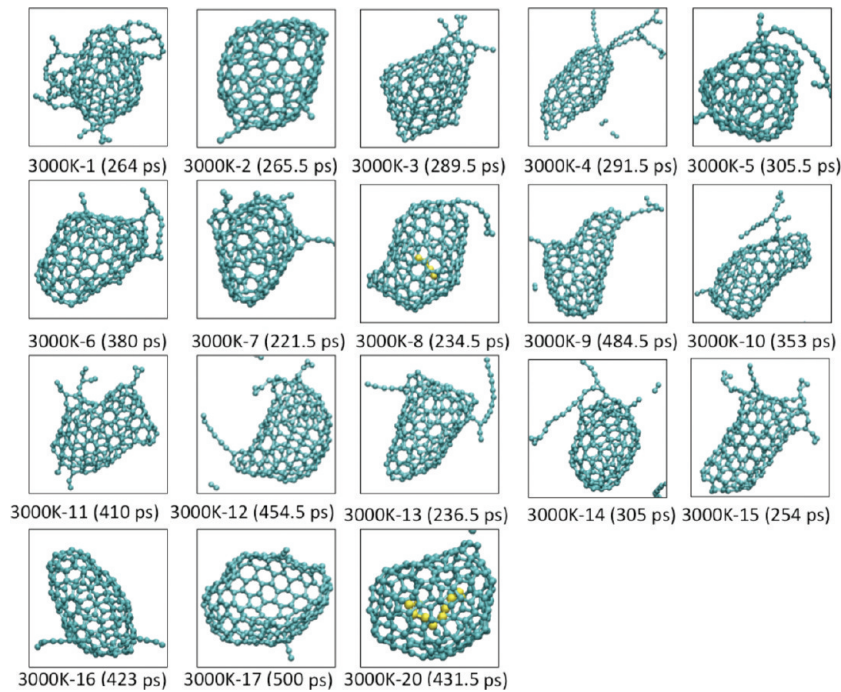


Figure 2. GF cages at 3000 K from the 18 successful trajectories. Yellow spheres indicate encapsulated fragments inside the formed cage.

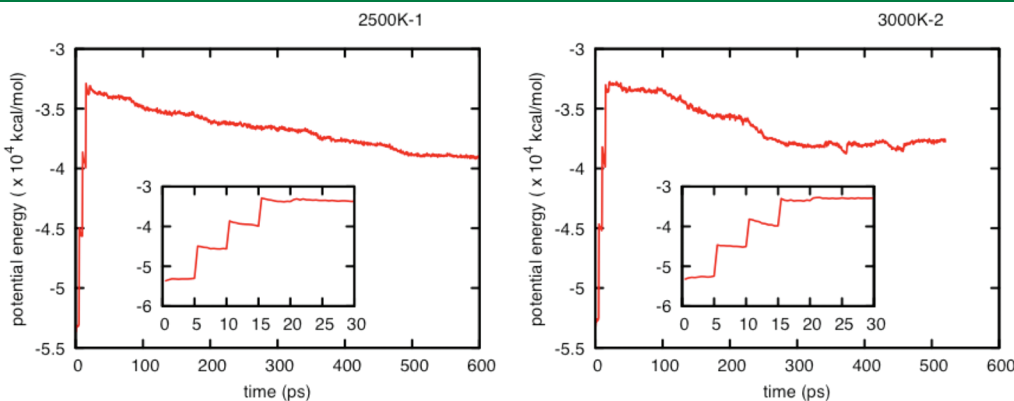


Figure 3. Potential energy variation curve during the course of 2500K-1 (left) and 3000K-2 (right) trajectories. The inset shows the early stage during the initial 30 ps. Jumps in energy correspond to hydrogen removals.

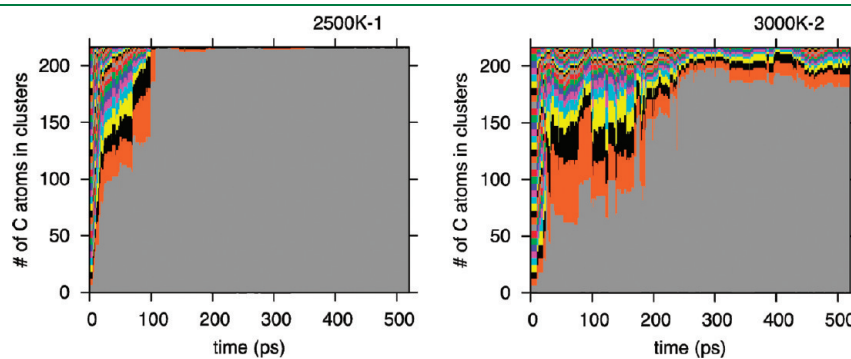


Figure 4. Cluster size ($\#C_{\text{cluster}}$) evolution during the course of 2500K-1 (left) and 3000K-2 (right) trajectories. There are 216 total carbon atoms, and the number of carbon atoms belonging to separate molecular clusters are indicated by vertical bars at a time interval of 1 ps. Initially, the reaction system contains 36 benzene molecules, and gradually small fragments coalesce into one major cluster (shown in gray).

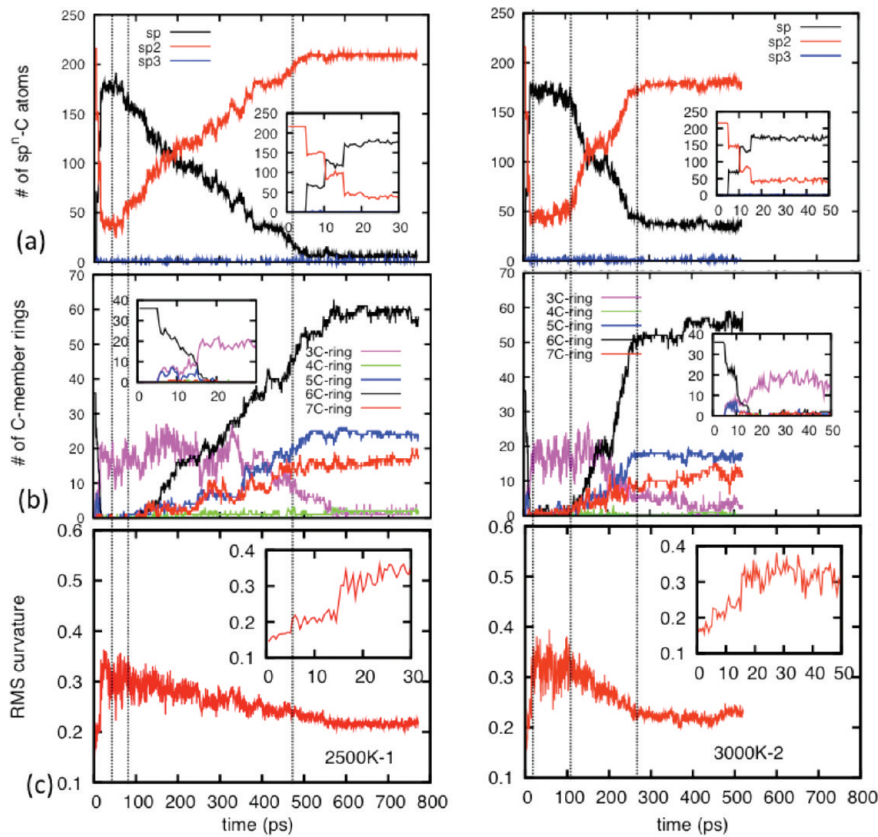


Figure 5. (a) Carbon hybridization count, (b) ring count statistics, and (c) root-mean-square curvature plot as a function of time during the course of trajectory 2500K-1 (left) and 3000K-2 (right).

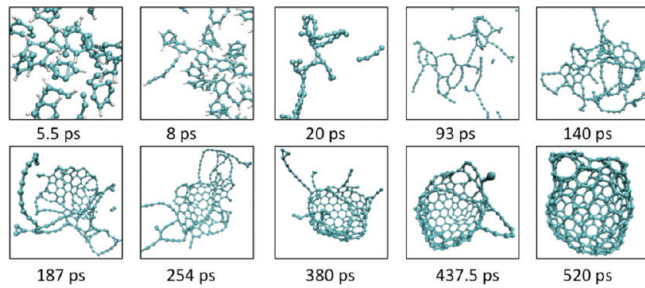


Figure 6. Key event snapshots at different stages in trajectory 2500K-1. Cyan and white spheres represent carbon and hydrogen atoms, respectively.

carbon atoms in the system. In ReaxFF/MD simulations, the largest clusters required a long time to coalesce with the smaller clusters after 20 ps.

As in our previous DFTB/MD study, we monitored the variations in the numbers of mono- or divalent (sp -hybridized), trivalent (sp^2 -hybridized), and tetravalent (sp^3 -hybridized) type carbon atoms as a function of simulation time. The curves are plotted in Figure 5a for trajectories 2500K-1 and 3000K-2. Since the number of tetravalent sp^3 carbons is always negligible under the conditions of the simulations, the plots record mainly the interconversion between sp and sp^2 carbons. Hence, the sp and sp^2 curves are roughly symmetric around 108 (half the number of totally available carbon atoms). In order to better understand and analyze the mechanism of the entire self-assembly process, we

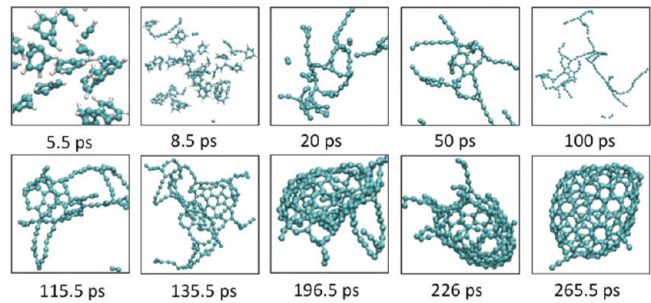


Figure 7. Key event snapshots at different stages in trajectory 3000K-2. Cyan and white spheres represent carbon and hydrogen atoms, respectively.

also plot in the same figures the variations in the number of carbon rings from triangles up to heptagons (Figure 5b) and the variation of RMS atomic curvature (Figure 5c) in the system. Three vertical dashed lines in all panels of Figure 5 indicate qualitatively stages in the self-assembly processes. Figures 6 and 7 present the key event snapshots at different stages for trajectories 2500K-1 and 3000K-2, respectively. The data from Figures 5–7 will be discussed in the following paragraphs.

III.B.2. Events during and after H Removal. Each H removal changed the coordination number of the carbon (from which H was abstracted) from three to two. Thus, each of the three initial H removal steps caused a sudden decrease in the total number of sp^2 carbons and the corresponding increase in the number of sp carbons, as can be seen in the insets of Figure 5a. Along with this

change in carbon hybridization, we observed a decrease in the number of hexagons, indicating ring-opening processes. Consequently, linear hydrocarbon chains were present in the system, for instance, shown in the snapshots at 8 ps in trajectory 2500K-1 (Figure 6) and at 8.5 and 20 ps in trajectory 3000K-2 (Figure 7). The ring-opening process producing linear polyacetylenic chains is similar to our observations in DFTB/MD simulations. Interestingly, several pentagons were created after the first H removal at 5 ps, but these pentagons disappeared quickly in the simulations at both temperatures. More significantly, around the same time, three-membered carbon rings ("triangles") started to appear in large numbers (approximately 20 per trajectory), reaching an abundance plateau at ~20 ps and *remaining the dominant ring species until 180–200 ps* (see insets of Figure 5b). Initially, triangles and pentagons were often created in an *m*-benzyne ring by bridge bond formation between the two hydrogen-devoid carbon atoms, forming bicyclo[3.1.0]hexatriene [see for instance the snapshots at 5.5 ps of trajectories 2500K-1 and 3000K-2 (Figures 6 and 7)]. This is an isomer of *m*-benzyne, which was speculated upon in the literature but shown in high-level *ab initio* quantum chemical calculations not to exist.³³ The pentagons of bicyclo[3.1.0]hexatriene were not stable and started to disappear from around 10 ps due to ring-opening processes, while the triangles continued to form abundantly, this time at the tails of polyyne chains and between the chains of Y-junction corners. Examples for such triangles at terminal or Y-junction positions are visible in snapshots of trajectory 2500K-1 at 20 and 93 ps (Figure 6) and 3000K-2 at 20 and 50 ps (Figure 7). In DFTB/MD simulations, triangles never appeared as stable species. Such carbon triangles were also discussed in a systematic ReaxFF benchmark study²⁸ and a ReaxFF/MD study of the aggregation of carbon in an atmosphere of hydrogen molecules.³⁴

As mentioned, the most noticeable difference between present ReaxFF/MD and previous DFTB/MD simulations concerns the time required for cage formation: ReaxFF/MD seems an order of magnitude slower to produce the first fully formed GF cages. The difference in time evolution is clearly visible in the time evolution of sp- and sp²-hybridized carbon when comparing ReaxFF/MD (Figure 5a) and DFTB/MD (Figure 3 in ref 15) results: Both simulations predict a minimum number of sp² carbon atoms after the third H removal, but it takes vastly longer in ReaxFF/MD simulations (20–30 ps in DFTB/MD, 150–200 ps in ReaxFF/MD) to recover and reach a 50:50 ratio to sp carbon atoms. At the same time, practically no polygonal rings were found at this stage, with the exception of the above-mentioned triangles. In this context, we note another important difference between DFTB/MD and ReaxFF simulation results: DFTB/MD simulations predicted that *ring-condensation processes* would occur rapidly once all hydrogen atoms left the system, easily bringing the number of hexagons back up to around the original number of 36. The same recovery process was found to be very slow in ReaxFF/MD simulations. It took roughly 450 ps (starting from ~45 to 500 ps) in the case of 2500K-1 and roughly 150 ps (from ~100 ps to ~250 ps) in the case of 3000K-2. Similarly as in the DFTB/MD simulations, hexagons were the dominant ring species, followed by pentagons and heptagons. As the ring condensation reactions continued in ReaxFF/MD simulations, the number of triangular carbons became gradually reduced. We conclude that the ring condensation process of pure carbon chains occurs on a different time scale with different intermediate ring species in the two methods. This difference may be explained

at least partially by the fact that the angle strain in linear carbon chains is overestimated by ~20% in ReaxFF relative to the quantum chemical B3LYP/6-31G(d) level of theory,²⁸ while the corresponding DFTB angle strain reproduces the first principles result well.

In Figure 5c, we trace the variation of the root-mean-square (RMS) of the atomic curvatures of all sp² carbon atoms in the system. It is clear that the RMS curvature has a small value (<0.2 Å⁻¹) for initial benzene rings at the simulated temperatures. Once the H removal began, the benzene rings started to open, and the molecules were transformed into linear fragments, which have larger flexibility, and thus larger local curvatures can be expected for sp² carbon atoms, for instance, at Y-junctions. During this stage, the curvature values were oscillating around a relatively large value > 0.3. Large oscillations in the curvature curve are attributed to the large flexibilities of Y-junction points during this stage. During the following ring condensation stage, the RMS curvature values slowly converged to values of the final cage structures.

Figure 8 displays the chemical composition of hydrocarbons (C_xH_y) before the second and third H removal step at 10 and 15 ps from all of the 20 trajectories at both temperatures. This figure corresponds to Figure 5 in ref 15. It is clear that at higher temperatures, the trajectories contain larger clusters. After 10 ps simulations, the largest cluster consisted of ~43 carbon atoms for T = 3000 K, whereas the largest cluster at T = 2500 K consisted of only ~36 carbon atoms; after 15 ps, the largest cluster was found to have ~170 carbon atoms at 3000 K but only ~130 at 2500 K. The clusters at both stages are mainly dominated by open-chain polyacetylene-like structures. In the case of DFTB/MD simulations, PAH species and fullerene precursors were already present at ~15 ps; in the case of ReaxFF/MD simulations, only polyacetylene-like chain structures were found. Similarly to DFTB/MD predictions, larger clusters tend to have slightly lower H/C ratios than the overall system's H/C ratio, while smaller fragments have somewhat higher H/C ratios.¹⁵

III.B.3. Cage Self-Assembly. The mechanism of dynamic fullerene self-assembly is qualitatively similar in both DFTB/MD and ReaxFF/MD simulations, with major differences concerning chemical reaction speed and differences in predicted intermediate structures as discussed above. The **first step** is the *ring-opening and fragmentation* process. In ReaxFF/MD simulations, during H removal, all carbon rings were destroyed, giving way to polyacetylene-like chains. In contrast to DFTB/MD simulations, this step continues beyond the last H removal (until ~20 ps). The **second step** in ReaxFF/MD simulations is the *linear chain growth process*. Short, linear carbon chains devoid of hydrogen fuse, creating larger linear and branched chains. This step is characteristic for the ReaxFF/MD simulations and does not occur during DFTB/MD simulations, where rings were formed already during H removal from ring-opened polyacetylene-like chains. The **third step** is dominated by *ring condensation*, starting from small nuclei of condensed rings. Hexagons are most abundant, while a significant number of pentagons provided enough positive curvature to the structure, causing the appearance of basket-shaped structures with linear polyyne chains attached ("octopus on the rock" structures). The number of heptagons is competitive with that of the pentagons but remains smaller. Since pure carbon chains are abundant in ReaxFF/MD simulations after H removal, the "arms of the octopus" are somewhat more abundant when compared to DFTB/MD simulations. Finally, the **fourth step** of fullerene cage self-assembly, *cage-closure*,

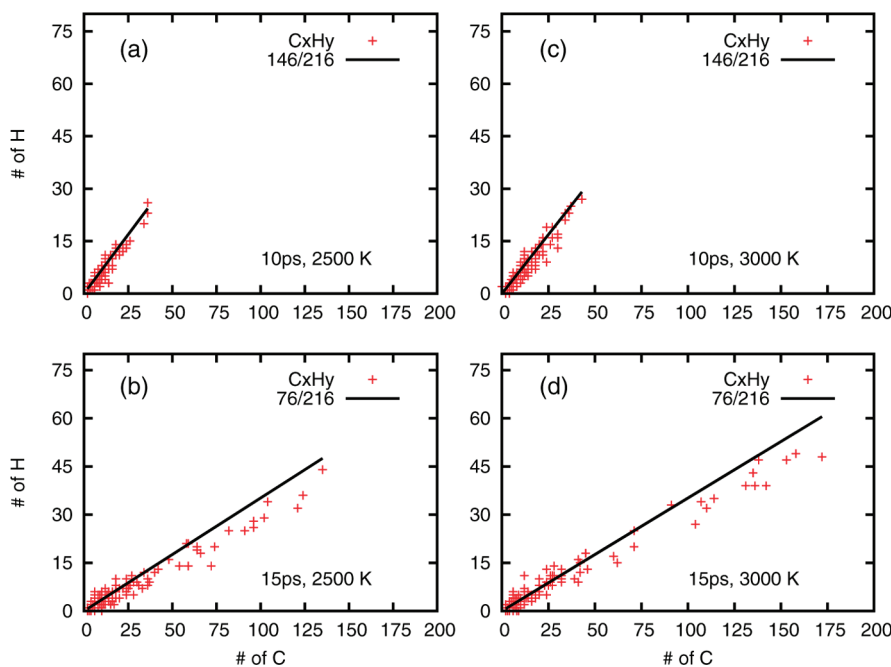


Figure 8. Hydrocarbon cluster compositions at (a) 10 ps for 2500 K, (b) 15 ps for 2500 K, (c) 10 ps for 3000 K, and (d) 15 ps for 3000 K (before the H removal steps). Each point corresponds to a C_xH_y species. The continuous lines represent the overall H/C ratio of the entire system. Data points are plotted for all 2500 K (left) and 3000 K (right) trajectories.

occurred during a drawn-out process and is shown in Figures 6 (520 ps) and 7 (265.5 ps). Similar to the DFTB/MD predictions, in the final closed cages, the numbers of hexagon rings were dominant, followed by around 20 pentagons and a comparable number of heptagons. Clearly, the final self-assembled cages are very large, highly defective, and far from obeying the isolated pentagon rule, similar as in DFTB/MD simulations.

III.C. Computational Efficiency. To accurately evaluate the differences in CPU times required for corresponding trajectories, we timed DFTB/MD and ReaxFF/MD simulations for a system with the following characteristics: 36 benzene molecules were placed in a 21 \AA^3 PBC box, and a Berendsen thermostat with 2500 K target temperature was employed in both simulations. For this benchmark, the time integration interval in DFTB was lowered to $\Delta t = 0.1$ fs so that we could estimate the performance difference of the two methods using the same number of time intervals for the same simulated time. A total of 1000 time integration steps were performed, yielding two trajectories of 100 fs length in both ReaxFF- and DFTB-based MD simulations. The CPU time required was 130.73 and 2396.31 s, respectively, on an Intel Xeon E5460@2.66 GHz CPU core, indicating that ReaxFF is roughly 20 times faster than DFTB in such a system. When taking into account that DFTB/MD simulations can be performed with a larger time interval of $\Delta t = 0.48$ fs (while still conserving total energy in NVE simulations with an error of only a few kcal/mol), the speedup of ReaxFF reduces effectively to a factor of about 4.

IV. SUMMARY AND CONCLUSIONS

ReaxFF/MD simulations predict similar patterns of fullerene formation during benzene combustion to those of previous DFTB/MD simulations,¹⁵ with major differences concerning chemical reaction speed and some differences in predicted

intermediate structures. Common to both methods is the prediction that, under the given carbon concentration in the absence of a carrier gas, giant fullerene cages with sizes between 155 and 212 (DFTB/MD: between 174 and 212) carbon atoms are formed in relatively high yields of 60% (2500 K, DFTB/MD: 50%) and 85% (3000 K, DFTB/MD: 42%). The cage self-assembly in both types of MD simulations involves the benzene ring-opening, carbon chain, and ring growth via ring-condensation reactions of sp²-hybridized carbon chains attached to sp³ carbon ring networks. In both simulations, hexagons finally outweigh by far pentagons and heptagons, and the final giant fullerene (GF) cages possess linear carbon chains attached to the cages at sp³ carbon defects. The major difference between classical ReaxFF and quantum chemical DFTB potentials concerns the reactivity of the partially hydrogenated and pure carbon species: DFTB predicts a much faster succession of events, leading to fullerene cage closure being up to a full order of magnitude faster (~ 50 ps vs ~ 500 ps) than ReaxFF. It appears that the bending of sp¹ chains is probably the deciding factor in the reaction: A comparison of the potential energy profiles for the bending of the C_3 molecule (see Figure S1 in the Supporting Information) shows that this mode is stiffer in ReaxFF than in the DFTB and DFT methods, even though ReaxFF outperforms DFTB in the prediction of isomer energies of the C_{28} species (Table S1 in Supporting Information). Further differences were found as follows:

- 1 Final cages often appear to be “nested” or “spiroid”-like in ReaxFF/MD simulations, exhibiting major discontinuities in the sp² carbon cage walls.
- 2 GFs occasionally exhibit endohedrally encapsulated small C_n chains or rings, different from previous DFTB/MD simulations.
- 3 In ReaxFF simulations, carbon triangles are common occurrences as termini of linear carbon chains and during hydrogen removal as part of the hypothetical bicyclo[3.1.0]hexatriene

- isomer of *m*-benzyne (see also Figure S1 in the Supporting Information).
- 4 In ReaxFF simulations, carbon rings open up to form linear chains during hydrogen removal.

It is difficult to pinpoint the exact contribution of these fundamental differences between both methods to each phenomenological difference. Since DFTB is an approximate method of density functional theory, which itself is an approximation of higher *ab initio* quantum chemical methods, we conclude that ReaxFF/MD is well suited to describe fullerene formation processes on nanosecond time scales. These simulations for the presented systems are between 4 and 20 times faster than corresponding quantum chemical DFTB/MD simulations, depending on the employed time integration intervals.

■ ASSOCIATED CONTENT

5 Supporting Information. Frozen potential energy scan of the $\angle CCC$ angle of the C₃ molecule in its singlet ground state using self-consistent-charge (SCC) and nonself-consistent-charge (NCC) DFTB levels of theory, ReaxFF, and B3LYP/6-311G(d); relative energies of C₂₈ isomers in electronvolts and corresponding linear regression coefficient R² for correlation between B3LYP/6-31G(d) and SCC- and NCC-DFTB, B3LYP/6-31G, AM1, PM3, and ReaxFF methods. Cartesian coordinates in Ångstroms of last snapshot structures from trajecories 1–20 at 2500 and 3000 K corresponding to either t_f or t_{end}, as indicated in Tables 1 and 2. In these structures, label C' denotes endohedrally encapsulated carbon atoms. This material is available free of charge via the Internet at <http://pubs.acs.org>.

■ AUTHOR INFORMATION

Corresponding Author

*E-mail: acv13@engr.psu.edu (A.C.T.v.D.); sirle@iar.nagoya-u.ac.jp (S.I.).

■ ACKNOWLEDGMENT

We thank Biswajit Saha for providing the initial g1 coordinates. S.I. acknowledges support by the Program for Improvement of Research Environment for Young Researchers from Special Coordination Funds for Promoting Science and Technology (SCF) commissioned by the Ministry of Education, Culture, Sports, Science and Technology (MEXT) of Japan. This work was supported in part by a CREST (Core Research for Evolutional Science and Technology) grant in the Area of High Performance Computing for Multiscale and Multiphysics Phenomena from the Japan Science and Technology Agency (JST).

■ REFERENCES

- (1) Kroto, H. W.; Heath, J. R.; O'Brien, S. C.; Curl, R. F.; Smalley, R. E. *Nature* **1985**, *318*, 162.
- (2) Krätschmer, W.; Fostiropoulos, K.; Huffman, D. R. *Chem. Phys. Lett.* **1990**, *170*, 167.
- (3) Howard, J. B.; McKinnon, J. T.; Makarovskiy, Y.; Lafleur, A. L.; Johnson, M. E. *Nature* **1991**, *352*, 139.
- (4) Heben, P.; Goel, A.; Howard, J. B.; Rainey, L. C.; Vander Sande, J. B. *Proc. Combust. Inst.* **2000**, *28*, 1397.
- (5) Frenklach, M. *Phys. Chem. Chem. Phys.* **2002**, *4*, 2028.
- (6) Alford, J. M.; Bernal, C.; Cates, M.; Diener, M. D. *Carbon* **2008**, *46*, 1623.
- (7) Goel, A.; Heben, P.; Vander Sande, J. B.; Howard, J. B. *Carbon* **2002**, *40*, 177.
- (8) *Masters of the Flame: Industrial Production of Fullerenes Becomes a Reality*; Nano-C: Westwood, MA, 2004.
- (9) Takehara, H.; Fujiwara, M.; Arikawa, M.; Diener, M. D.; Alford, J. M. *Carbon* **2005**, *43*, 311.
- (10) Homann, K.-H. *Angew. Chem., Int. Ed.* **1998**, *37*, 2434.
- (11) Pope, C. J.; Marr, J. A.; Howard, J. B. *J. Phys. Chem.* **1993**, *97*, 11001.
- (12) Ahrens, J.; Bachmann, M.; Baum, T.; Griesheimer, J.; Kovacs, R.; Weilmünster, P.; Homann, K. H. *Int. J. Mass. Spectrosc. Ion Proc.* **1994**, *138*, 133.
- (13) Grieco, W. J.; Howard, J. B.; Rainey, L. C.; Vander Sande, J. B. *Carbon* **2000**, *38*, 597.
- (14) Richter, H.; Labrocca, A. J.; Grieco, W. J.; Taghizadeh, K.; Lafleur, A. L.; Howard, J. B. *J. Phys. Chem. B* **1997**, *101*, 1556.
- (15) Saha, B.; Shindo, S.; Irle, S.; Morokuma, K. *ACS Nano* **2009**, *3*, 2241.
- (16) Irle, S.; Zheng, G.; Elstner, M.; Morokuma, K. *Nano Lett.* **2003**, *3*, 1657.
- (17) Irle, S.; Zheng, G.; Wang, Z.; Morokuma, K. *J. Phys. Chem. B* **2006**, *110*, 14531.
- (18) Zheng, G.; Irle, S.; Morokuma, K. *J. Chem. Phys.* **2005**, *122*, 014708.
- (19) Yamaguchi, Y.; Maruyama, S. *Chem. Phys. Lett.* **1998**, *286*, 336.
- (20) Maruyama, S.; Yamaguchi, Y. *Chem. Phys. Lett.* **1998**, *286*, 343.
- (21) Powles, R. C.; Marks, N. A.; Lau, D. W. M. *Phys. Rev. B* **2009**, *79*, 075430.
- (22) Irle, S.; Zheng, G.; Elstner, M.; Morokuma, K. *Nano Lett.* **2003**, *3*, 465.
- (23) Huang, J. Y.; Ding, F.; Jiao, K.; Yakobson, B. I. *Phys. Rev. Lett.* **2007**, *99*, 175503.
- (24) Chenoweth, K.; van Duin, A. C. T.; Goddard, W. A. *J. Phys. Chem. A* **2008**, *112*, 1040.
- (25) Page, A. J.; Moghtaderi, B. *J. Phys. Chem. A* **2009**, *113*, 1539.
- (26) van Duin, A. C. T.; Dasgupta, S.; Lorant, F.; Goddard, W. A. *J. Phys. Chem. A* **2001**, *105*, 9396.
- (27) Clar, E. *Polycyclic Hydrocarbons*; AP: London, 1964.
- (28) Nielson, K. D.; van Duin, A. C. T.; Oxgaard, J.; Deng, W.-Q.; Goddard, W. A. III. *J. Phys. Chem. A* **2005**, *109*, 493.
- (29) Brenner, D. W. *Phys. Rev. B* **1990**, *42*, 9458.
- (30) Brenner, D. W. *Phys. Rev. B* **1992**, *46*, 1948.
- (31) Tersoff, J. *Phys. Rev. B* **1988**, *37*, 6991.
- (32) Bogana, M.; Ravagnan, L.; Casari, C. S.; Zivellonghi, A.; Baserga, A.; Bassi, A. L.; Bottani, C. E.; Vinati, S.; Salis, E.; Piseri, P.; Barborini, E.; Colombo, L.; Milani, P. *New J. Phys.* **2005**, *7*, 1.
- (33) Kraka, E.; Anglada, J.; Hjerpe, A.; Filatov, M.; Cremer, D. *Chem. Phys. Lett.* **2001**, *348*, 115.
- (34) Lümmen, N. *Comput. Mater. Sci.* **2010**, *49*, 243.